

A NONVOLUME PRESERVING PLASTICITY THEORY  
WITH APPLICATIONS TO POWDER METALLURGY\*

Brice N. Cassenti  
United Technologies Research Center  
East Hartford, Connecticut 06108

ABSTRACT

A plasticity theory has been developed to predict the mechanical response of powder metals during hot isostatic pressing. The theory parameters were obtained through an experimental program consisting of hydrostatic pressure tests, uniaxial compression and uniaxial tension tests. A nonlinear finite element code was modified to include the theory and the results of the modified code compared favorably to the results from a verification experiment.

INTRODUCTION

In the Hot Isostatic Pressing (HIP) process a sheet metal container is fabricated in the approximate shape of a component to be manufactured. The container is evacuated, filled with a powder metal and sealed. The container is then placed in a HIP facility where it is subjected to high temperatures and pressures. For powder metals consisting of nickel base superalloys typical HIP temperatures are 1150C at pressures of 1000 atm. During the HIP all the void space is squeezed out from between the particles. After HIP the container is removed and the solid component remains.

---

\* Work performed as a part of AFOSR Contract F49620-78-C-0090

The HIP process is ideally suited to the manufacture of turbine and compressor disks in jet engines and is cost competitive with forging. Unfortunately the final shape of the hot isostatic pressed component is not a photographic replica of the original container shape. Non-photographic distortions are introduced by several sources. Some of these include: intrinsic differences in the stiffness of the container at different locations, and distortions due to gravitational loading. The cost for constructing components by HIP could be substantially reduced if the final shape of the component resulting from a given container shape could be predicted.

The permanent volume reductions inherent to the HIP process, of about 35 percent, cannot be predicted by classical plasticity theory, which assumes no permanent volume changes. Therefore classical plasticity theory must be modified to include permanent volume changes. Additionally, volume reductions of 35 percent imply linear strains of 10 to 15 percent and therefore large strain measures must be employed.

There have been previous attempts, Refs. 1-9, to describe the deformation mechanics of powder metals, but none of these has been successfully applied to the prediction of the final shape of hot isostatic pressed components.

A nonvolume preserving plasticity theory has been developed for this purpose. The parameters for the theory were found through the execution of an experimental program. The theory was added to the MARC\* computer code. The computer code was used to model a simple verification experiment and the

---

\* MARC Analysis Research Corporation

results predicted by the code compared favorably to the results of the experiment. Each of the above topics will be discussed in the following sections.

#### ACKNOWLEDGEMENTS

The author would like to acknowledge Dr. David Parks for his help in developing the plasticity theory and especially for the development of Eqs. (14) through (19). The author would also like to thank Dr. Kenneth Cheverton for his aid in defining the early stages of the program.

#### PLASTICITY THEORY

A finite strain plasticity theory requires: (1) specification of a yield surface to delineate regions of elastic and plastic response, (2) a hardening rule for the expansion of this yield surface, and (3) a flow rule for relating stress and strain increments. This flow rule must be formulated using large strain, stress and stress rate measures. Each of these topics will be considered separately below.

#### Yield Surface Formulation

A yield surface can be developed based on heuristic arguments. Since the powder particle orientation is random, the powder aggregate should initially respond isotropically. Thus the yield function must be an isotropic function and depend on only the stress through its three invariants. Also, yielding must occur under hydrostatic pressure and the yield function must approach that of a metal as densification progresses. Since invariant

$I_1$  is a linear multiple of the hydrostatic component of stress, and yield surfaces for metals are usually defined in terms of invariant  $J_2$ , which is the second invariant of the deviatoric stress tensor, both of these invariants must appear in the yield function

$$f = f(I_1, J_2, J_3, h_\alpha) = 0 \quad (1)$$

where the third invariant,  $J_3$ , of the deviatoric stress tensor has been included for completeness, and

$$I_1 = \sigma_{KK}$$

$$J_2 = 1/2 S_{ij} S_{ij}$$

$$J_3 = 1/6 \epsilon_{ijk} \epsilon_{lmn} S_{il} S_{jm} S_{kn} \quad \text{is the determinant of the deviatoric stress tensor}$$

$$S_{ij} = \sigma_{ij} - 1/3 \delta_{ij} \sigma_{kk} \quad \text{is the deviatoric stress tensor, and}$$

$\sigma_{ij}$  is the stress tensor

$\delta_{ij}$  is the Kronecker delta

$\epsilon_{ijk}$  is the permutation tensor

The parameters  $h_\alpha$  were determined experimentally and depend on deformation measures,  $\eta_\alpha$ .

Assume that a HIP powder metal has unequal responses in tension and compression, and that the yield surface has no sharp corners. A simple yield function satisfying the above assumptions is

$$\beta^2 \left( \frac{I_1 + \alpha}{3} \right)^2 + J_2 = \sigma_o^2 / 3 \quad (2)$$

A yield function of the form of Eq. (2) has previously been proposed by Green in Ref. 4, Shima and Oyane in Ref. 7, and Kuhn and Downey in Ref. 8. Equation

(2) is an ellipse in  $I_1, \sqrt{J_2}$  space (Fig. 1), with deformation dependent parameters,  $\alpha, \beta$  and  $\sigma_0$ . The yield surface is plotted in principal stress space with  $\sigma_3$  zero in Fig. 2, for the case  $\alpha = 0$ .

A large strain theory of plasticity based on Eq. (2) can be developed by decomposing the symmetric part of the velocity gradient tensor,  $D_{ij}$  into elastic and plastic parts, or

$$D_{ij} = \frac{1}{2} \left( \frac{\partial v_i}{\partial x_j} + \frac{\partial v_j}{\partial x_i} \right) = D_{ij}^e + D_{ij}^p \quad (3)$$

The plastic deformation rate  $D_{ij}^p$  is assumed to be given by an associated flow rule

$$D_{ij}^p = \dot{\lambda} \frac{\partial f}{\partial \sigma_{ij}} \quad (4)$$

Where  $\dot{\lambda}$  is a scalar function greater than zero. The choice of the deformation parameters,  $\eta_\alpha$ , and the specification of the flow rule will be discussed in the following two sections.

#### Choice of Hardening Deformation Parameters

In this section, strain hardening of a compacting metal powder is discussed and parameters to characterize hardening are identified. This is necessary to complete the specification of the plastic deformation. Initially, the yield surface of the powder aggregate will be small. During the compaction and sintering process yield strength will grow and the yield surface will expand. Compaction alone will cause growth of the yield surface along only the  $I_1$  axis (Fig. 1) with a theoretical limit corresponding to full densification. Yield stress in shear will be less affected by compaction. Additionally, yield strength will grow

in all directions of stress space with increased sintering time. Thus, there exists a time dependent hardening phenomenon unique to powder metallurgy. Since plastic deformations are assumed to occur instantaneously, time enters the plasticity theory as a parameter defining yield surface size at the time of plastic deformation.

The process of strain-hardening in triaxial pressure will primarily be a geometric effect on the microscopic scale. There could also be a contribution to the apparent macroscopic hardening due to real strain hardening of the particles as they experience large plastic shearing deformations. Such an effect could raise the effective yield strength of the metal particles. The separate contributions of matrix hardening and void reduction can be determined from systematic experiments using different initial volume fractions.

Initially, powder particles contact each other at isolated points. As pressure is applied, the contact areas and the powder stiffness increase. The macroscopic result is strain hardening of the powder due to macroscopic shrinkage. In the limit the powder is completely compacted and the response to further pressure increments is elastic dilation; the plastic bulk modulus has become infinite.

An obvious choice for a deformation measure,  $\eta_1$ , is the void volume fraction. The void volume fraction is a measure of the macroscopic shrinkage and should reflect an increase in stiffness due to an increase in contact area between the individual particles, or

$$\eta_1 = v \quad (5)$$

The void volume fraction does not represent any permanent changes that occur during plastic deformation. If as in classical plasticity theory the effective

plastic strain is used this would not represent all of the permanent deformations since permanent volume changes would not be represented. A third deformation measure, the plastic volume change would then be required.

Rather than use the permanent volume change and the effective plastic strain as two independent deformation measures, a single measure, the plastic work, would be sufficient to represent both effects. Therefore, let

$$\eta_2 = W^P = \int_0^t \sigma_{ij} D_{ij}^P dt \quad (6)$$

In classical volume preserving plasticity theory using either the plastic work or the effective plastic strain produces exactly the same result. The plastic work, or equivalently the inelastic energy dissipation has been used previously to describe nonlinear material response, for example, in Refs. 9 and 10.

#### Development of Flow Rule

It is now possible to describe the symmetric part of the velocity gradient tensor,  $D_{ij}$  in terms of the stress rate, for small strains, using Hooke's Law for the elastic response and Eq. (4) for the plastic response in the form

$$\dot{\sigma}_{ij} = L_{ijkl}^{e.p} D_{kl} = L_{ijkl}^{e.p} \dot{\epsilon}_{kl} \quad (7)$$

where for small strains

$$D_{kl} = \dot{\epsilon}_{kl} \quad (8)$$

In general the yield function is of the form

$$f(\sigma_{ij}, h_\alpha) = 0 \quad (9)$$

where elastic deformations occur when  $f < 0$  and plastic deformations occur when  $f = 0$  and where  $h_\alpha$  are parameters in the yield surface dependent on deformation history measures  $\eta_\beta$ , or

$$h_\alpha = h_\alpha (\eta_\beta)$$

Assume that the plastic deformations are given by an associated flow rule

$$\dot{\epsilon}_{ij}^p = \lambda \frac{\partial f}{\partial \sigma_{ij}} \quad (10)$$

Using Hooke's law for the elastic deformations

$$\dot{\epsilon}_{ij}^e = \frac{1}{E} (1+\nu) \dot{\sigma}_{ij} - \nu \sigma_{kk} \delta_{ij} \quad (11)$$

the total strain rate can be written as

$$\dot{\epsilon}_{ij} = \dot{\epsilon}_{ij}^e + \dot{\epsilon}_{ij}^p \quad (12)$$

Equation (9) can be equivalently written as

$$\dot{f} = \frac{\partial f}{\partial \sigma_{ij}} \dot{\sigma}_{ij} + \frac{\partial f}{\partial h_\alpha} \frac{\partial h_\alpha}{\partial \eta_\beta} \dot{\eta}_\beta = 0 \quad (13)$$

In Ref. 11, Parks has shown that

$$\dot{\eta}_\beta = \dot{\lambda} k_\beta \quad (14)$$

where

$$(\dot{\phantom{x}}) = \partial(\phantom{x})/\partial t \quad (15)$$

The quantity  $k_1$  can be determined from

$$\dot{\eta}_1 = \dot{\nu} = (1-\nu) D_{kk} = \dot{\lambda} k_1 \quad (16)$$

and  $k_2$  can be found from

$$\dot{\eta}_2 = \dot{W}^p = \sigma_{ij} D_{ij}^p = \dot{\lambda} k_2 \quad (17)$$

For the yield surface of Eq. (2), from Ref. 11

$$k_1 \approx \frac{2}{3} (1-\nu) \beta^2 (I_1 + \alpha) \quad (18)$$

$$k_2 = \frac{2}{3} \left[ \sigma_o^2 - \alpha \beta^2 \left( \frac{I_1 + \alpha}{3} \right) \right] \quad (19)$$

Equations (7) through (13) can be solved to give

$$\begin{aligned}
L_{ijkl}^{e.p} = \frac{E}{1+\nu} & \left\{ \delta_{ik} \delta_{jl} - \frac{\frac{\partial f}{\partial \sigma_{ij}} \frac{\partial f}{\partial \sigma_{kl}}}{\frac{\partial f}{\partial \sigma_{mn}} \frac{\partial f}{\partial \sigma_{mn}} - \left(\frac{1+\nu}{E}\right) H} \right. \\
& + \left(\frac{\nu}{E}\right) \frac{\left[ \delta_{ij} - \frac{\frac{\partial f}{\partial \sigma_{mm}} \frac{\partial f}{\partial \sigma_{ij}}}{\frac{\partial f}{\partial \sigma_{mn}} \frac{\partial f}{\partial \sigma_{mn}} - \left(\frac{1+\nu}{E}\right) H} \right] \left[ \delta_{kl} - \frac{\frac{\partial f}{\partial \sigma_{nn}} \frac{\partial f}{\partial \sigma_{kl}}}{\frac{\partial f}{\partial \sigma_{mn}} \frac{\partial f}{\partial \sigma_{mn}} - \left(\frac{1+\nu}{E}\right) H} \right]}{\frac{1-2\nu}{E} + \left(\frac{\nu}{E}\right) \left[ \frac{\frac{\delta f}{\delta \sigma_{mm}} \frac{\delta f}{\delta \sigma_{nn}}}{\frac{\partial f}{\partial \sigma_{mn}} \frac{\partial f}{\partial \sigma_{mn}} - \left(\frac{1+\nu}{E}\right) H} \right]} \right\} \quad (20)
\end{aligned}$$

where

$$H = \frac{\partial f}{\partial h_\alpha} \frac{\partial h_\alpha}{\partial \eta_\beta} k_\beta \quad (21)$$

The quantities  $\frac{\partial h_\alpha}{\partial \eta_\beta}$  are hardening parameters which are determined from the mechanical test results and described in the section on Material Property Determination. A more detailed discussion of the plastic flow rule can be found in Ref. 12.

#### Large Strain Flow Rule Considerations

Following McMeeking and Rice, Ref. 13, when using the current deformed state as the reference configuration, all stress measures coincide. However, the rates associated with these stress measures do not coincide. A stress rate which is useful for expressing large deformation constitutive laws is the Jaumann, or corotational rate (Ref. 14). The Jaumann rate of Cauchy stress is

$$\overset{\nabla}{\sigma}_{ij} = \dot{\sigma}_{ij} - \sigma_{ip} \Omega_{pj} + \Omega_{ip} \sigma_{pj} \quad (22)$$

where  $\dot{\sigma}_{ij}$  is the material time rate of Cauchy stress  $\sigma_{ij}$  and

$$\dot{\Omega}_{ij} = \frac{1}{2} (\partial v_i / \partial x_j - \partial v_j / \partial x_i)$$

The constitutive law of interest is of the form

$$\dot{\sigma}_{ij} = L_{ijkl} D_{kl} \quad (23)$$

where  $L$  denotes the rate moduli,  $D_{ij}$  is the symmetric part of the velocity gradient tensor.

$L_{ijkl}$  is developed in Ref. 15 for large strains as

$$L_{ijkl} = L_{ijkl}^{e.p} - \frac{1}{2} \left[ \delta_{ik} \sigma_{jl} + \delta_{jk} \sigma_{il} + \delta_{il} \sigma_{jk} + \delta_{jl} \sigma_{ik} \right] + \sigma_{ij} \delta_{kl} \quad (24)$$

and  $L_{ijkl}^{e.p}$  is the small strain elastic-plastic stiffness in Eq. (21). The tensor  $L_{ijkl}$  is not symmetric due to the presence of the last term, or

$$L_{ijkl} \neq L_{klij}$$

For a hydrostatic pressure

$$\sigma_{ij} = P \delta_{ij}$$

the tensor is symmetric and since this should be the primary part of the loading during the HIP process, the last term should produce a nearly symmetric stiffness. It, therefore, was decided to separate the last term into symmetric and unsymmetric parts, and add the symmetric part to the stiffness matrix and transfer the unsymmetric part to the loading side of the governing equations.

## MATERIAL PROPERTY DETERMINATION

To predict the mechanical response of metal powder subjected to the HIP process it is necessary to know the mechanical properties of the metal during the HIP cycle. These mechanical properties can be obtained by removing test specimens from the HIP facility at various stages in a HIP cycle. The partial HIP samples would represent the powder at various stages for a pressure-temperature history. A complete description of the mechanical properties can then be obtained by postulating yield surfaces, flow rules, hardening laws and creep properties and comparing these predictions to the results of mechanical tests on the partial HIP samples.

### Partial HIP Tests

The UTRC HIP facility has been utilized to process powder metals through temperature-pressure-time profiles closely paralleling the procedure used to fabricate full size turbine disks to near net shape.

The HIP facilities allow several partial HIP samples to be preheated simultaneously. Since the powder is initially weak a container is required to retain the powder shape for temperatures exceeding 2000 F (1100 C). Therefore, all specimens were preheated at 2000 F (1100 C) and 1 atm for 12 hr. During the preheat cycle the powder is encapsulated in quartz and attains sufficient strength from sintering to be handled. During the preheat the density changed from 60 to 65 percent of full density initially to 65 to 70 percent of full density upon completion of the cycle.

After the completion of the preheat cycle the samples have the quartz container removed and a glass container substituted. At HIP temperatures the inside surface of the glass container fuses with the outer powder metal particles and forms a gas tight seal about the powder metal, and the glass has no strength or stiffness. Consequently, a uniform hydrostatic stress is transmitted to the powder metal. The glass container with the preheated or sintered powder metal is next placed in the HIP facility and subjected to a specified temperature, pressure time cycle.

A set of tests was performed at 1800 F (982 C) and various pressure, with the maximum temperature and pressure acting for 10 minutes only. These tests successfully produced partially dense samples. The test regime was expanded to include 1600 F (871 C), 1900 F (1638 C) and 2000 F (1093 C) at appropriate pressures and again the time at maximum temperature and pressure was held to 10 min.

Some understanding of the compaction process can be obtained by applying the hydrostatic pressure plastic compaction model (Ref. 16), where the yield pressure was represented by

$$\frac{P}{\sigma_y} = \frac{2}{3} \left[ -\ln\left(\frac{v}{v_i}\right) - \left(1 - \frac{v}{v_i}\right)^2 \ln v_i + a \left(\frac{v}{v_i}\right) \left(1 - \frac{v}{v_i}\right) \right] \quad (25)$$

$$a = \frac{C v_i}{(1-v_i) \tan^2 \theta} - 1 \quad (26)$$

and

$$\cos \theta = \frac{\rho_i}{4} + \sqrt{\left(\frac{\rho_i}{2}\right) \left(\frac{1 + \rho_i}{8}\right)} \quad , \text{ and} \quad (27)$$

where  $v_i$  = the initial void volume fraction

$\rho_i = 1 - v_i$  is the initial relative density, and

$C \approx 2.75$

In order to apply the model the yield stress of the powder particle material must be known. This data does not exist and therefore the short time partial HIP data has to be reduced to determine the yield stress. For each of the temperatures, 1600 F (871 C), 1800 F (982 C) and 2000 F (1093 C), the yield stress was estimated and Eq. (25) was applied to determine the relative density for various applied pressures. Figure 3 presents the results of the calculations and demonstrates good agreement for the yield stresses given by

$$\sigma_y = \left(1.1 \times 10^9 \text{ ksi}\right) e^{-\frac{T}{120.7 R}} = \left(7.58 \times 10^{12} \text{ nt/m}^2\right) e^{-\frac{T}{67 K}} \quad (28)$$

Equation 28 results in yield stresses that are somewhat low for superalloys. Three facts could account for this: (1) the yield stress for the pre-HIP powder metal is generally lower than for the fully consolidated powder, (2) the strain rate during a partial HIP cycle is relatively slow and therefore produces a somewhat lower effective yield stress, and (3) the creep rates at high temperatures are relatively high, producing an apparently lower yield stress.

#### Mechanical Tests

To determine the shape of the yield surface several types of mechanical tests are required. Each type of test produces one point on the yield surface. There is one point on the surface that is known: the hydrostatic

pressure of the HIP process. A compression test performed at temperature will provide a second point on the yield surface and will also provide some information on the elastic, hardening and plastic flow of the material. Tension tests performed at temperature, when compared to a compression test performed at temperature, will determine the symmetry of the yield surface. The compression tests are the most important tests to be performed since they produce a hydrostatic pressure which is the predominant loading feature during a HIP cycle. Two deformation measures will be used to characterize the yield surface; the void volume fraction and the plastic (nonrecoverable) work. Therefore, the measurement of the axial length change is not sufficient to determine the mechanical response and a measurement of the volume will also be required. The final volume of a compression specimen was measured after a completed test but this does not provide a complete description of the path to the final state.

More than thirty compression tests were performed. Three of these tests were used to size the compression specimens and determine the test conditions. The remaining tests were all completed in a similar manner. The specimens consisted of a right circular cylinder 0.5 in (.127 cm) long by 0.2 in. (0.51 cm) in diameter. Each specimen was placed in a furnace in an inert gas and brought up to the temperature at which the specimen was hot isostatically pressed. At temperature the specimen was subjected to compression crosshead displacement rate of 0.0025 in./min (0.00635 cm/min) and the load was recorded. After the load leveled out, the crosshead rate was doubled to 0.005 in./min (0.00127 cm/min).

The average values for the height, diameter, and volume change measurements are presented in Table 1 along with the standard deviations. From the last column in Table 1 it can be seen that over all the samples there was a significant decrease in the height and a significant increase in the diameter, while there was essentially no change in the volume.

A total of 14 tensile tests were completed and resulted in significantly lower yield stress values than the compression tests, especially at 2000 F (1093 C). The low tensile yield stresses could be a result of the presence of voids which would be adjacent to the particle interfaces. Tensile stresses, which are amplified at the void, would tend to separate the particles producing a smaller apparent yield than compression stresses which would tend to close the voids. Microscopic examination and room temperature tensile tests (Ref. 14), indicated the powder was not contaminated.

The uncertainty associated with the tensile test results necessitated the use of the experimental observation that the volume was conserved during compression.

#### Interpretation of Mechanical Test Results

The mechanical tests indicated that there is little or no volume change in compression. Coupling this fact with the hydrostatic pressure yield stress,  $P_y$ , and the compressive yield stress  $\sigma_c$  will determine all of the yield parameters in Eq. (9) as

$$\alpha = \sigma_c \quad (29)$$

$$\beta^2 = \frac{3}{q} \quad (30)$$

$$\sigma_o = \sigma_c \quad (31)$$

where

$$q = \frac{3 P_y}{\sigma_c} - 1 \quad (32)$$

The experimental results for the tensile yield stress,  $\sigma_T$ , were not reliable but can be determined from Eq. (2) as

$$\sigma_T = \left( \frac{q^2 - 1}{q^2 + 1} \right) \sigma_c \quad (33)$$

Normalizing the compressive yield stress data,  $\sigma_c$ , with respect to the initial powder particle yield stress,  $\sigma_y$ , shows that this ratio is approximately a linear function of relative density as shown in Fig. 4, or

$$\frac{\sigma_c}{\sigma_y} = b \left( \frac{v_i - v}{1 - v_i} \right) \quad (34)$$

where  $P_y$  is evaluated from Eq. (61) by setting P equal to  $P_y$

$v$  is void volume fraction

$v_i$  is initial void volume fraction, and

$b$  can be determined by requiring the tensile yield stress to vanish at the initial void volume fraction, or

$$\sigma_T = 0 \text{ at } v = v_i$$

From Eqs. (32) and (33), the above condition on  $b$  is

$$\lim_{v \rightarrow v_i} \frac{P_y}{\sigma_c} = \frac{2}{3} \quad (35)$$

Then from Eqs. (25) and (34)

$$b = \frac{C}{\tan^2 \theta} \quad (36)$$

where  $\theta$  is given by Eq. (27) and  $C \approx 2.75$ .

The temperature,  $T$ , and strain rate,  $\dot{\epsilon}$ , dependence have been included in the initial particle yield stress,  $\sigma_y$ . A good fit occurs when

$$\sigma_y = \sigma_{y_0} e^{-\frac{T}{T_0}} \left[ 1 + \alpha \ln \left( \frac{\dot{\epsilon}}{\dot{\epsilon}_0} \right) \right] \quad (37)$$

for uniaxial stress conditions.

A good fit to the specimens partially densified in the HIP facility occurs if

$$\dot{\epsilon} \approx 0.00315/\text{min.}$$

The parameters in Eq. (37) are

$$\sigma_{y_0} = 1.074 \times 10^{10} \text{ kis } (7.41 \times 10^{13} \text{ nt/m}^2)$$

$$T_0 = 120.7 \text{ R } (67.06 \text{ K})$$

$$\alpha = 0.03403, \text{ and}$$

$$\dot{\epsilon}_0 = 8.148 \times 10^8 / \text{min.}$$

Equations (29) through (37) are the plastic formulation added to the MARC code, and are compared to the experimental measurements in Figs. 3, 4, and 5. The agreement is good if the volumetric creep under hydrostatic pressure is included (Fig. 3). Volumetric creep will move points subject to HIP for more than 10

min (the solid symbols in Fig. 3) to the right of the line representing instantaneous plastic deformation.

Although little work hardening was observed during the compression tests, it may have an influence on the final deformations, and therefore an approximate hardening law of the form of Eq. (38) below was assumed.

$$\sigma_c = b \left( \frac{v-v_i}{1-v_i} \right) \sigma_y \left[ 1 - a_1 e^{-a_2 W^P} \right] \quad (38)$$

where  $W^P$  is the plastic work,  $a_1$ ,  $a_2$  are constant work hardening parameters.

From the uniaxial compression tests it was noted that the compressive yield stress seems to level off at about 1.4 times the initial compressive yield stress and therefore the constant  $a_1$  is given by

$$a_1 = 0.286 \quad (39)$$

The constant  $a_2$  was found to vary with temperature approximately by the relation

$$\frac{1}{a_2} = \begin{cases} C_2 \left( \frac{T_c - T}{\Delta T_o} \right) & T \leq T_c \\ 0 & T \geq T_c \end{cases} \quad (40)$$

where  $C_2 = 9090 \text{ psi} \left( 6.26 \times 10^6 \frac{\text{nt}}{\text{m}^2} \right)$

$$T_c = 2020 \text{ F} \text{ (1104 C)}$$

$$\Delta T_o = 420 \text{ F} \text{ (216 C)}$$

A more complete discussion of the work hardening evaluation is given in Ref. 14.

The elastic constants are required to complete the formulation but only Young's modulus can be derived from the compression test data. The Young's

Modulus, E, was assumed to be linear function of void volume fraction, v, and an exponential function of temperature, T, given below

$$E = E_1 e^{-\frac{T-T_0}{T_1}} \left( \frac{v_i - v}{v_i} \right) \quad (41)$$

where  $v_i$  is the initial void volume fraction, and  $E_1$ ,  $T_0$  and  $T_1$  were chosen to provide a good fit to the data, as

$$E_1 = 1.5 \times 10^6 \text{ psi}$$

$$T_0 = 1900 \text{ F (1038 C)}$$

$$T_1 = 163 \text{ F (72.8 C)}$$

Figure 6 compares the analytical expression with the resulting mechanical test data. The comparison is within the experimental error. Since it was not possible to measure radial deflections during the testing, Poisson's ratio could not be determined.

It should be noted that if the tensile strengths were accurately measured, a yield surface utilizing: the hydrostatic yield pressure, the compression yield stress, the tension yield stress and the fact that volume was preserved during compression, could have been taken as

$$\beta^2 \left( \frac{I_1 + \alpha}{3} \right)^2 + J_2 \left\{ 1 + \gamma \left( 1 + \frac{9 J_3}{2\sqrt{3} J_2^{3/2}} \right) \right\} - \frac{\sigma_0^2}{3} = 0 \quad (42)$$

where  $\beta$ ,  $\alpha$ , and  $\sigma_0$  are given by Eqs. (29-31), and

$$\gamma = \frac{1}{2} \left\{ \left( \frac{\sigma_c}{\sigma_T} \right)^2 - 1 - \frac{\left( \frac{\sigma_c}{\sigma_T} + 1 \right)^2}{\left( \frac{3 P_y}{\sigma_c} - 1 \right)^2} \right\} \quad (43)$$

and  $J_3$  is the third invariant of the deviatoric stress tensor

Note that if  $\sigma_T$  is given by Eq. (33) the parameter  $\gamma$  vanishes.

With the experimental specification of the parameters the yield surface is completely determined.

## MODEL VERIFICATION

### Verification Criteria

The validation tests were designed to avoid duplication of the uniform hydrostatic stress state of the partial HIP tests. The experiments must therefore result in a nonvanishing shear stress within the sintered material. A nonhydrostatic stress state can be achieved with the application of the uniform external pressure if the material has nonhomogenous properties. This may be achieved by imbedding in the metal powder a different material, for example, steel spheres or fully compacted powder spheres or cylinders. Such an experimental configuration will produce a nonhydrostatic stress state and will make use of existing hardware and techniques. Metal foil could be placed tangent to a steel sphere and the resulting displacements measured and compared to the predicted displacements.

### Plastic Analysis for Spherical Inclusions

Before proceeding with the verification experiments, a finite element

model of the experiment was analyzed using a version of the MARC code modified to include the powder metal constitutive properties of 7 axisymmetric elements illustrated in Fig. 7. Constraints were set to insure only spherically symmetric radial displacement would result. The steel sphere was modeled as rigid, and therefore the radial displacements were fixed in the powder at the surface of the steel sphere. The analysis considered only the plastic deformations that would result in raising the external pressure to 1000 atm. In Fig. 8, the model resulted in predictions that the void volume fraction decreased near the sphere or the density is highest near the sphere. At an applied external pressure of 1000 atm all points in the specimen are more than 90 percent of full density. The deflections of the foil can be easily calculated using the radial displacements and are presented as a function of the distance from the center of the foil, as shown in Fig. 8. At about 8 ksi (533 atm) the edge of the foil should be nearly flat. These conditions had been run during the partial HIP tests and produced a relative density of about 0.85, which agrees with the predicted results presented in Fig. 8,

#### Verification Results

The specimen design consists of a steel sphere imbedded in a sintered rod. A layer of nickel foil is placed tangent to the sphere. One, two, or three sphere and nickel foil configurations are placed within the sintered bar. Figure 9 illustrates a typical configuration. The first verification experiment consisted of a test to insure the configuration would HIP properly and was successfully completed.

Two sintered bars were hot isostatic pressed, based on the above success and the finite element results for a maximum of 10 min at 1800 F, (982 C) and 8 psi (533 atm). These bars contained a total of five 0.25 (0.63 cm) diameter spheres.

Foil displacement measurements were successfully obtained from three of the five spheres and the results of these measurements are presented in Fig. 10, along with the prediction from the finite element model.

The lack of agreement near the center may be due to either the relative elasticity of the sphere and powder including thermal effects, which were not modeled, or due to the weight of the sphere. The rapid decrease in error with position indicates the error may be due to the elastic effects. Another source for the difference can be attributed to the fact that the foil and the upper and lower bar segments may not have been in contact and gradually brought into contact as the HIP progressed. The numerical predictions and the experimental measurements agree to within the accuracy of the experiment, and verify that an accurate mechanical description of the powder response has been developed.

## CONCLUSIONS

In the analysis developed, classical plasticity theory has been extended to include the large permanent changes in volume of about 30 percent that are incurred during HIP. The theory developed assumes an isotropic yield surface and uses an associated flow rule. The assumed yield surface includes all three invariants of the stress tensor although presently the yield surface

only uses the first invariant of the stress tensor, and the second invariant of the deviatoric stress tensor.

The parameters in the theory were obtained through an experimental program consisting of hydrostatic pressure tests, uniaxial compression and uniaxial tension tests. From the hydrostatic pressure tests a simple analytical expression was developed that predicted the change in density as a function of pressure and temperature. Results of the compression tests indicated that there is no measurable change in volume in compression and that the compression yield stress is a linear function of void volume fraction. The uniaxial tension tests were inconclusive and the results were used for comparison with prediction from the theoretical model only.

Isotropic hardening of the yield surface was assumed to depend on void volume fraction and plastic work accumulated. Experimental results showed that the primary dependence was on void volume fraction.

A nonlinear finite element code was modified to include the plasticity theory and an experiment was run to verify the theory and the code modifications. The verification experiment consisted of steel spheres imbedded in partially dense bars of powder metal. Each of the spheres had a layer of foil placed tangent to the sphere. The bar, with spheres and foil, was placed in a furnace and subjected to a pressure loading of 8 ksi (533 atm) at 1800° F. The resulting distortion of the foil was measured and compared to the results of a finite element analysis using the modified code. The numerical prediction and the experimental measurements agreed to within the accuracy of the experiment.

As a result a modified finite element code exists capable of predicting the mechanical reponse of powder metals and is now being applied to predict the final shape of components manufactured by the HIP process.

#### REFERENCES

1. Wilkinson, D. S. and Ashby, M. F., "The Development of Pressure Sintering Maps," Sintering and Catalysis Materials Science Research, Vol. 10, G. C. Kuczynski, Ed., Plenum Press, 1975, pp. 473-492.
2. Ramquist, L., "Theories of Hot Pressing, Power Metallurgy," Vol. 9, No. 17, 1966, pp. 1-25.
3. Torre, C., "Berg-Hutterman, Montash, Montan," Hochschule Loeben, Vol. 93, 1948, p. 62.
4. Green, R. J., "A Plasticity Theory for Porous Solids," International Journal for Mechanical Sciences," Vol. 14, 1972, pp. 215-224.
5. Suh, N. P., "A Yield Criterion for Plastic, Frictional, Work-Hardening Granular Materials," International Journal of Powder Metallurgy, Vol. 5, 1969, pp. 69-87.
6. Needleman, A., "Void Growth in an Elastic Plastic Medium," Journal of Applied Mechanisms," Vol. 38, 1972, pp. 964-970.
7. Shima, S. and Oyane, M., "Plasticity Theory for Porous Metals," International Journal of Mechanical Science, Vol. 18, 1976, pp. 285-291.
8. Kuhn, H. A. and Downey, C. L., "Deformation Characteristics and Plasticity Theory of Sintered Powder Materials," Internal Journal of Powder Metallurgy, Vol. 7, 1971, pp. 15-25.
9. Corapcioglu, Y. and Uz, T., "Constitutive Equations for Plastic Deformation of Porous Materials," Powder Technology, Vol. 21, 1978, pp. 269-274.
10. Bodner, S. R. and Partom, Y., "Constitutive Equations for Elastic-Visco Plastic Strain Hardening Materials," Journal of Applied Mechanics, Transation of the ASME, pp. 385-389, June 1975.
11. Parks, D. M., "Finite Deformation Plasticity Formutation for Compacting Metal Powders," Communication to B. N, Cassenti, dated March 25, 1979.

REFERENCES (Cont'd)

12. Cassenti, B. N., "Analytical Modeling of the Hot Isostatic Pressing Process," AFOSR-TR-81, Air Force Office of Scientific Research, Bolling Air Force Base, Washington, D. C., July 1980.
13. McMeeking, R. M. and Rice, J. R., "Finite-Element Formulations for Problems of Large Elastic-Plastic Deformation," International Journal of Solids and Structures, Vol. 10, 1974, pp. 321-339.
14. Prager, W., "Introduction to Mechanics of Continua," Ginn and Co., Boston, 1961.
15. Nagtegaal, J. C. and deJong, J. E., "Some Computational Aspects of Elastic-Plastic Large Strain Analysis," MARC Analysis Research Corporation, Palo Alto, California.
16. Cassenti, B. N., "The Manufacture of Disks by the Hot Isostatic Pressing Process," AIAA Paper No. 80-1111, AIAA/SAE/ASME 16th Joint Propulsion Conference, June 30 - July 2, 1980, Hartford, CT.

TABLE 1

STATISTICAL GEOMETRY CHANGES FOR  
COMPRESSION TESTS

Ratio, Final/Initial	Mean m	Std. Dev. s	$\frac{m-1}{s}$
Height	0.9345	0.029	-2.25
Diameter	1.0330	0.010	3.31
Volume	0.9975	0.015	-0.17

TABLE 2

RESULTS OF ROOM AND HIGH TEMPERATURE TENSILE TESTS

Specimen No.	Relative Density	Room Temperature Yield Stress (ksi) 0.2 Percent	Room Temperature Ultimate Stress (ksi)	Yield Stress (ksi) at 1800 deg. F
1004	0.990	144	168	0.022
1098*	0.900	-	82.4	0.126
1114	0.977	102	156	2.30
1115	0.984	138	164	-

\* Failed in grip

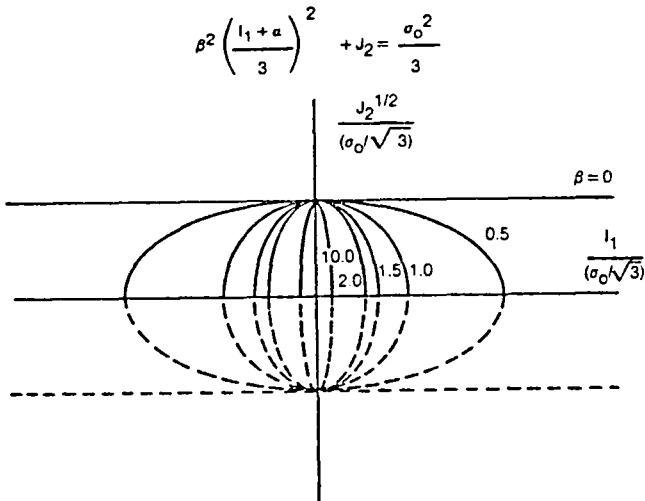


Fig. 1. Assumed yield surface in  $I_1, J_2^{1/2}$  stress space for  $\alpha=0$

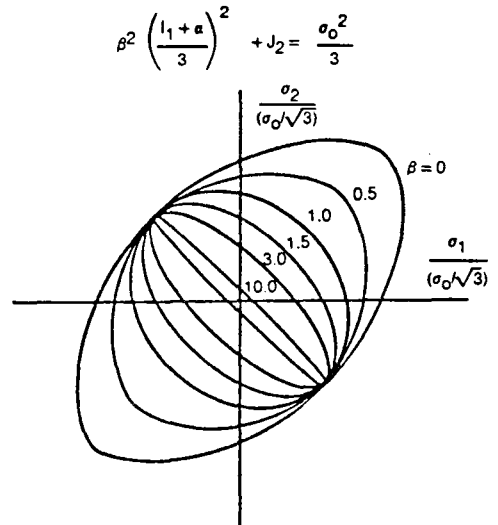


Fig. 2. Assumed yield surface in principal stress space for  $\sigma_3=0, \alpha=0$

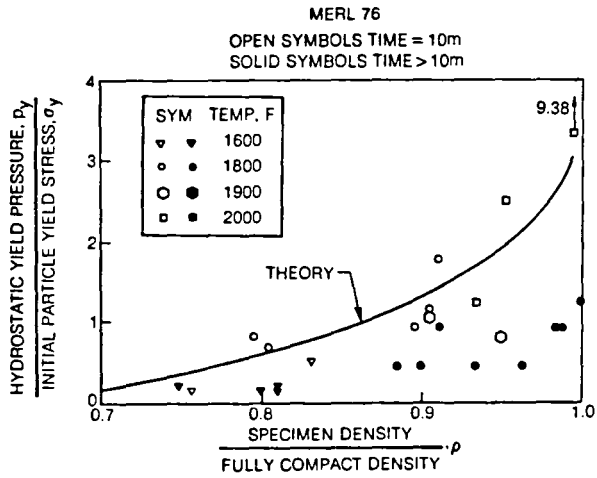


Fig. 3. Hydrostatic yield pressure test results

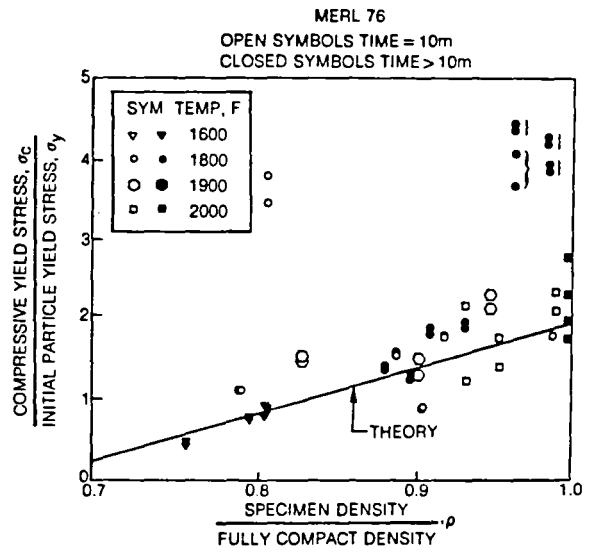


Fig. 4. Compressive yield stress results

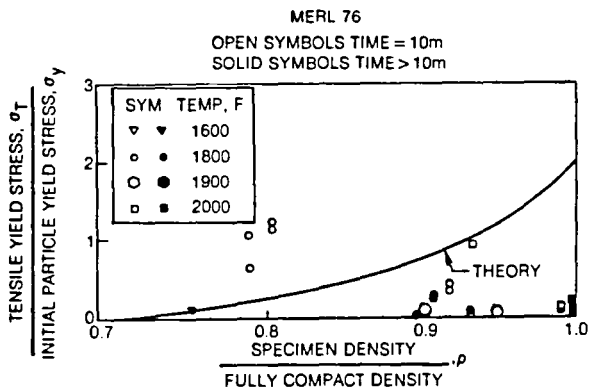


Fig. 5. Tensile yield stress results

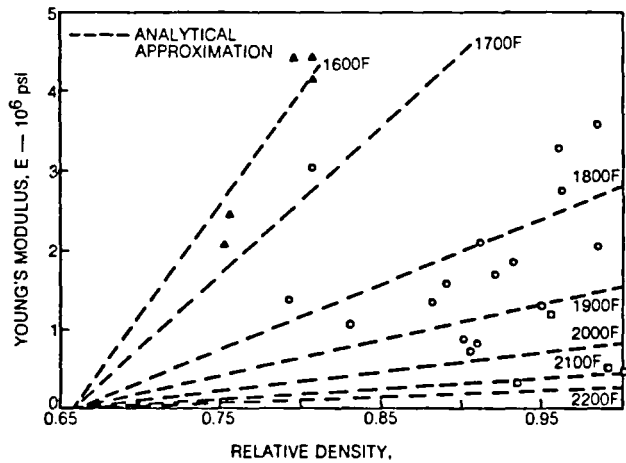


Fig. 6. Young's modulus for partially dense MERL 76

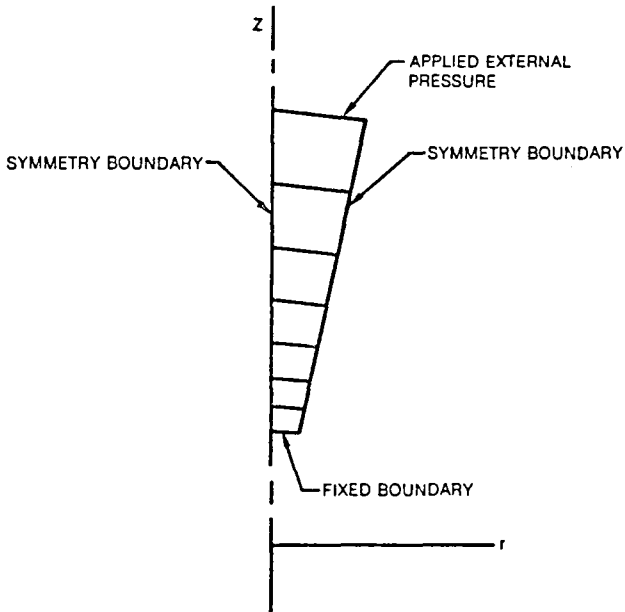


Fig. 7. Verification experiment finite element model

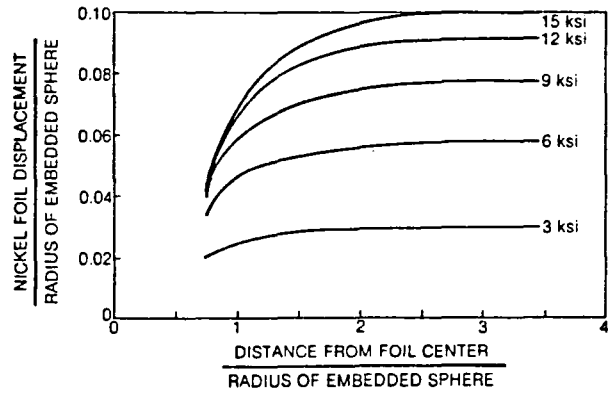


Fig. 8. Predicted nickel foil displacement for verification experiment

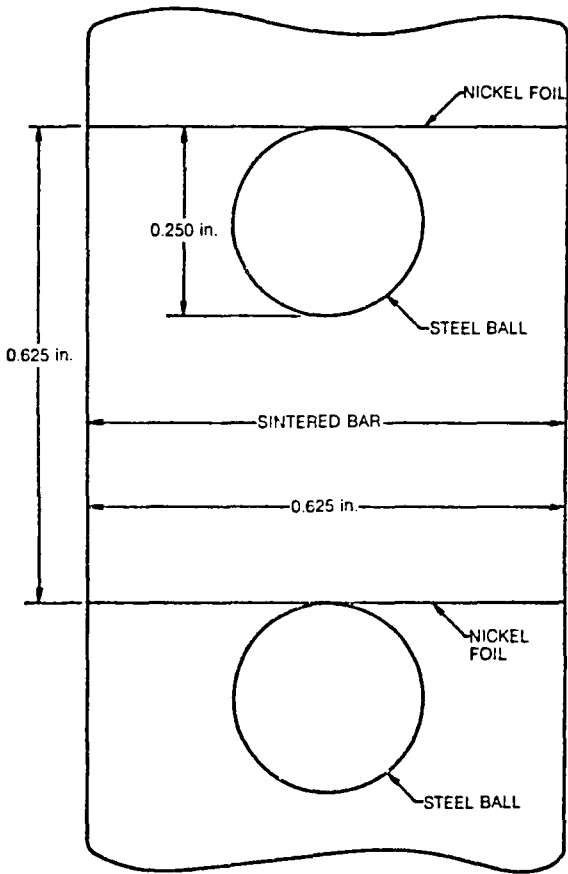


Fig. 9. Typical configuration of verification experiment

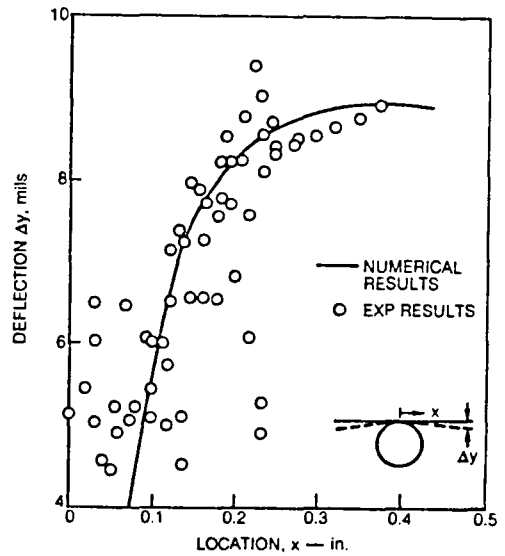


Fig. 10. Verification experiment